Muons to Probe Tectonic Activity

Ojaswi Gupta
Roll No: MS14058

A dissertation submitted for the partial fulfilment
of BS-MS dual degree in Science

Under the guidance of
Dr. Satyajit Jena

April 2019

Indian Institute of Science Education and Research Mohali
Sector - 81, SAS Nagar, Mohali 140306, Punjab, India

Dedicated to my brother, parents and friends.

Certificate of Examination

This is to certify that the dissertation titled **Muons to Probe Tectonic Activities** submitted by **Ojaswi Gupta** (Reg. No. MS14058) for the partial fulfillment of BS-MS dual degree programme of the Institute, has been examined by the thesis committee duly appointed by the Institute. The committee finds the work done by the candidate satisfactory and recommends that the report be accepted.

Dr H K Jassal | Dr Ananth Venkatesan | Dr Satyajit Jena (Supervisor)

Dated: 26.04.2019

Declaration

The work presented in this dissertation has been carried out by me under the guidance of Dr. Satyajit Jena at the Indian Institute of Science Education and Research Mohali.

This work has not been submitted in part or in full for a degree, a diploma, or a fellowship to any other university or institute. Whenever contributions of others are involved, every effort is made to indicate this clearly, with due acknowledgement of collaborative research and discussions. This thesis is a bonafide record of original work done by me and all sources listed within have been detailed in the bibliography.

Ojaswi Gupta
(Candidate)

Dated: April 26, 2019

In my capacity as the supervisor of the candidate's project work, I certify that the above statements by the candidate are true to the best of my knowledge.

Dr. Satyajit Jena
(Supervisor)

Acknowledgement

I would like to thank my thesis supervisor Dr. Satyajit Jena, without whose help and supervision, this thesis would have never been possible. I would also like to thank IISER Mohali for providing me with the resources and opportunities throughout the coursework.
Dr. Parth Chauhan has been a great mentor and guide and I can never thank him enough for all the help that he has given me over the years. I would also like to thank Dr Harvinder Kaur Jassal and Dr Ananth Venkatesan for being in my thesis evaluation committee and for providing useful inputs for the project.
My sincere thanks to Inayat for being my friend and to always motivate me to do better. I was extremely lucky to have amazing friends here. Animesh, Nilotpal, Jorawar, Abhinay, Vassu, Paras, Rohit bhaia, Nishat di, Kartik bhaia, Abin, Balu, Jain, Aswathy, Adheena, Awani thanks for all the support. Special thanks to Devwrat Dube for introducing me to quizzing and Abhijit for being the best team partner and support that one could have.
A big thanks to Dr Kirandeep Kaur for proofreading and providing corrections for the thesis.
Last but not the least, there are no words to thank the people who actually made it possible for me to do all this and everything else. Thanks and gratitude for my parents and my brother for everything. I am what I am because of you.

Ojaswi Gupta
MS14058
IISER Mohali

Do not go gentle into that good night,
Old age should burn and rave at close of day;
Rage, rage against the dying of the light.
Though wise men at their end know dark is right,
Because their words had forked no lightning they
Do not go gentle into that good night.
Good men, the last wave by, crying how bright
Their frail deeds might have danced in a green bay,
Rage, rage against the dying of the light.
Wild men who caught and sang the sun in flight,
And learn, too late, they grieved it on its way,
Do not go gentle into that good night.
Grave men, near death, who see with blinding sight
Blind eyes could blaze like meteors and be gay,
Rage, rage against the dying of the light.
And you, my father, there on the sad height,
Curse, bless, me now with your fierce tears, I pray.
Do not go gentle into that good night.
Rage, rage against the dying of the light.

Dylan Thomas

List of Figures

Contents

Abstract

This project is an attempt to observe the events happening at the sun and within the earth's atmosphere and to analyze their effects on muon flux and other incoming radiation. It has been observed that on several occasions, electronic appliances suddenly stop functioning at the same time in certain regions. This is a result of magnetic disturbance in the region which acts as an EMP (Electro Magnetic Pulse). This disturbance is caused by the huge mass of charged particles that are ejected by sun during Coronal Mass Ejection event in form of solar flares. This is accompanied by formation of sun spots on the surface of the sun. Earth is constantly bombarded with charged particles incident on the planet incoming from outer space, with majority of particles coming from the sun. These incoming particles from sun contribute towards Cosmic ray radiation. Therefore, the solar cycle may changes the flux of muon over the region of earth. These Cosmic Rays have the potential to cause far reaching changes to the atmosphere of the planet among other things.

Changes in the flux of this radiation is mainly caused due to events taking place at the sun in the form of solar activity which includes solar flares, sun spots, Radiation flux, magnetic changes etc. In this project we are trying to find out the effects of these phenomena on the muon flux incident on earth along with any effects caused due to atmospheric changes on earth itself.

We use the observations of these incoming disturbances and investigate any correlation with the tectonic activity of earth. The occurrence of the two events were compared by statistical tests to look for similarities in the pattern of the time series data.

Chapter 1

Introduction

1.1 Cosmic Rays

Scientist Victor Hess discovered cosmic rays in 1912 and even after a century later we do not fully understand them. Cosmic rays are the incoming particles that arrive on earth from outer space. They enter the Earth's atmosphere and interact with other particles or undergo decay while travelling on their path. These are mainly ionized nuclei comprising of $\sim 90\%$ protons, 9% helium nuclei (alpha particles) and rest heavier nuclei. These rays travel with speeds close to the speed of light and are hence relativistic. In less prominent cases some particles have been observed with ultra-relativistic energies of the order of 10^{20} eV. Cosmic rays are divided into two classes: "primary", the particles generated from astrophysical sources and "secondary", the particles created as a result of primaries interacting with interstellar gas. Protons, electrons, Helium, Oxygen etc. are examples of primary particles where as Lithium, Beryllium and Boron are secondaries. In fact, antiprotons and positrons are also considered to be secondary.

1.2 Solar Origins

Sun is the largest source of low energy cosmic rays on earth, releasing large amount of cosmic rays in form of solar flares and coronal mass ejections. The energy range for solar cosmic rays is about $\sim 10^7$ to 10^9eV. The composition of these cosmic rays is similar to the composition of sun with a large proportion of flux being protons.

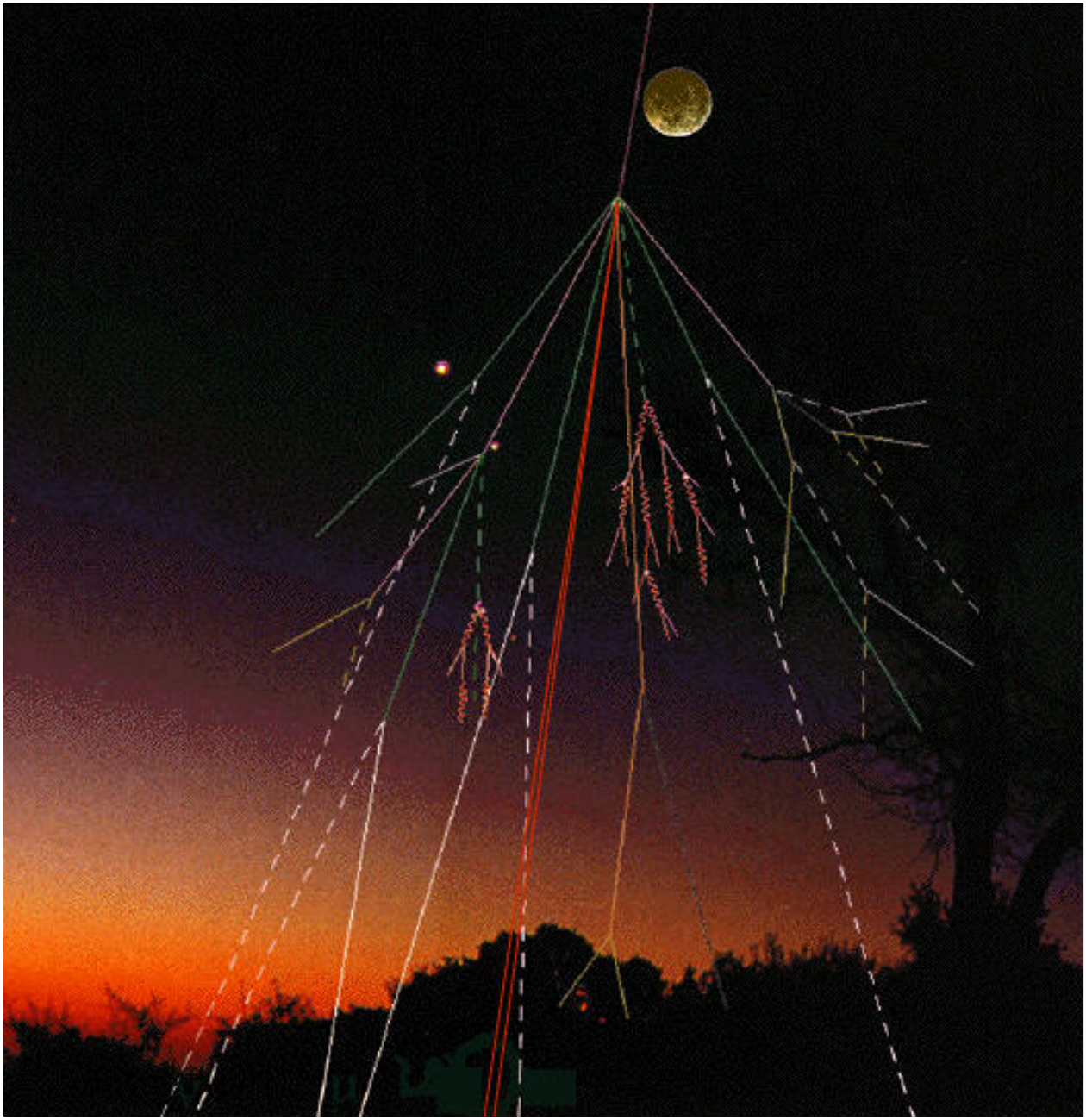

Figure 1.1: Incoming cosmic radiation in earth's atmosphere.(Courtesy of Dr. Joe Lykken, Deputy Director of Fermilab for Research)

1.3 Cosmic Ray Energy Spectrum

The energy spectrum of all the particle in cosmic rays can be easily be described by a single power law as shown in Figure1.2 with a small bend at about 3 PeV energies which is called as the "*knee*". Upto the knee region, the majority of Galactic cosmic ray flux is identified to be Supernovae remnants. According to standard picture the knee is believed to be caused due to a decreased flux of protons and He nuclei. But several experiments have claimed to find evidence of the knee being caused by heavier nuclei as compared to Helium. Towards the end of the spectrum at $4 \times 10^9 GeV$ energy, another feature which is called as "*ankle*" emerges.[Mon16]

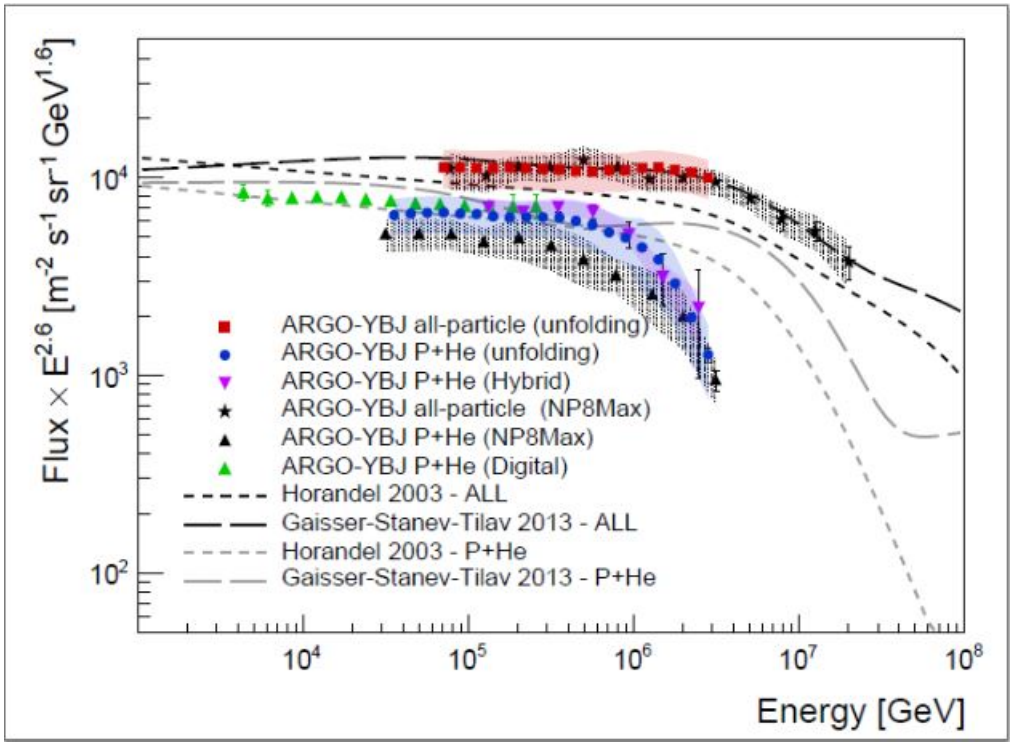

Figure 1.2: Cosmic ray energy spectrum showing proton + Helium flux as measured by ARGO-YBJ.Digital data is shown in green, Analog data obtained using Bayesian technique is in red and blue, Analog data via energy reconstruction is via a solid black triangle and a star. Dashed lines represent proton + helium spectrum according to the displayed Models[Mon16].

1.4 Muons

A muon, denoted by the Greek letter μ, is an elementary particle like an electron with a -1 charge and 1/2 spin, but much greater mass than an electron. It is also classified as a lepton owing to the belief that a muon has no sub-structure. The mass of a muon is $105.658 MeV/c^2$, about 207 times of that of an electron. Mean lifetime of a muon is just $(2.1969811 \pm 0.0000022)\mu s$ but its decay is a slow process due to muons undergoing decay by weak interactions instead of the more powerful strong interactions. Moreover the mass difference between a muon and its decay products is not very large therefore it also has a lower number of kinetic degrees of freedom available for decay.

$$\mu^- \rightarrow e^- + \bar{v}_e + v_\mu$$

$$\mu^+ \rightarrow e^+ + \bar{v}_\mu + v_e$$

Shown above is the most dominant form of muon decay, also known as Michel decay (after Louis Michel). Also it is interesting to note that because muons travel at a speed very close to the speed of light in vacuum, the effects of time dilation are observed. In spite of their very short lifetime almost 50% of measured radiation on earth is composed of muons. Time dilation equation[Ein05]:

$$\Delta t' = \Delta t \times \gamma = \frac{\Delta t}{\sqrt{1 - \frac{v^2}{c^2}}} \tag{1.1}$$

1.4.1 Muon Sources

Muons that are observed on earth are actually decay products of incoming heavier cosmic ray particles. Most abundant form of muon production is decay of secondary mesons. The most prominent pathways are shown as follows:

$$K^0 \rightarrow \pi^+ + \pi^-$$

$$\pi^+ \rightarrow \mu^+ + v_\mu$$

$$\pi^- \rightarrow \mu^- + v_\mu$$

Here kaons are created as byproducts of proton-proton collisions of heavier nuclei. A pion has a mass of 139.57 MeV and a muon has a mass of 105.66 MeV so energy released in production of a muon is 33.91 MeV.

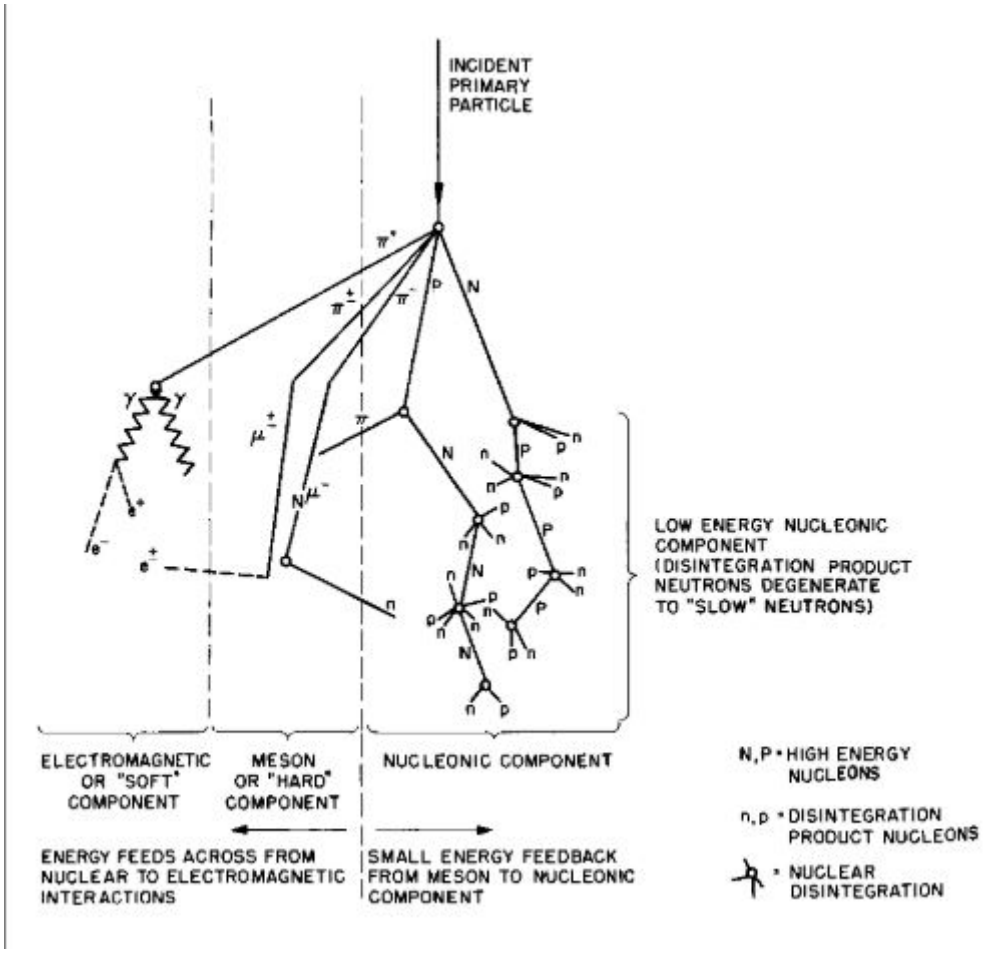

Figure 1.3: A typical cosmic ray air shower representing production and annihilation of particles along the way[Nce12].

1.5 Air Showers of Cosmic Radiation

When primary cosmic rays enter earths atmosphere, they interact extensively with the atoms and molecules present in the atmosphere and produce secondaries which then continue on their path towards earth. Whenever a primary particle hits a nucleus present in the air, it produces several energetic hadronic particles. These hadronic particles then quickly decay to form several other secondaries like, X- rays, muons, protons, anti-protons etc[AK77]. Once the collision between primaries and atmospheric particles happens, pions are created (in majority) and neutral pions decay to create photons:

$$\pi^0 \rightarrow \gamma + \gamma$$

These photons then form an electromagnetic cascade by creating further more particles like protons, neutrons, photons, antiprotons etc.

Chapter 2

Earth

2.1 Geomagnetism

The magnetic field of celestial bodies has been a very curious phenomenon to humans for thousands of years. Probably one of the major reasons is the non-uniformity in the magnetic field; for example, the moon has no magnetic field and mars has an ever-changing and field with different strengths in the two hemispheres. Here we will look at the magnetic field of earth and the interplanetary magnetic field that surrounds the planet. This magnetic field acts as a protective blanket for the planet and covers earth from incoming cosmic radiation and solar winds. Moreover, on the planet it has been used for fundamental processes like navigation, another example is Avian Magnetotaxis where birds use the earth's magnetic field's direction and strength to navigate their path. We have known about the presence of this field for thousands of years, and yet there is no complete understanding of the process. The currently accepted model for the geomagnetic field is the Dynamo Theory which will be described in the next section.

2.2 Dynamo Theory

The magnetic field of the earth is generated as a result of the movement of the fluid present in its outer core. This fluid is formed of magnetically charged metallic elements which on rapid movement produce magnetic fields. It is proposed that during the formative ages of a planet, the heavier metallic particles tend to move towards the core of the planet while the lighter particles rise to form the crust of the planet. The dynamo process can be considered

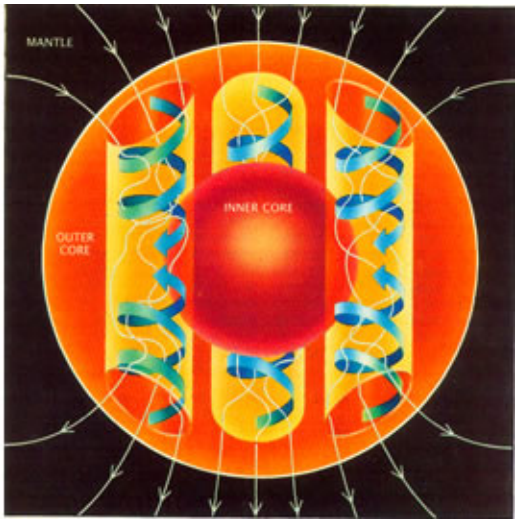

Figure 2.1: Illustration of earth dynamo process, the convection currents lead to circulating electric currents which then generate earth's magnetic field. (Courtesy: Wikipedia.org)

merely to be a form of instability. It is these instabilities that provide a system with new degrees of freedom of motion. A crucial aspect of the dynamo process is that new state that emerges from an unstable state has not only a difference in the degree of freedom but also one more characteristic-"magnetic field". Magnetic fields are generated by the fluid motion in the core which can be represented mathematically as follows:

$$\frac{\partial}{\partial t}B - \bigtriangledown \times (\lambda \bigtriangledown \times B) = \bigtriangledown \times (v \times B) \tag{2.1}$$

here λ is the magnetic diffusivity and is defined as $\lambda = (\mu\sigma)^{-1}$. σ is the electrical conductivity and μ is magnetic permeability of the fluid.

As this is a theory of instabilities, there are no sufficient general conditions that exist for a dynamo process to occur. Some necessary conditions must be met though, which are given in the following statements:

1. $Re \equiv V_o r_o/\lambda > \pi$, Here V_o is maximum velocity inside the fluid sphere. Re is the critical Reynolds number and r_o is the radius of the sphere.

2. Cowlings theorem states that growing axisymmetric or two-dimensional solutions of equation 2.1 do not exist. A most important result of this theorem is that successful dynamos are unable to possess a high degree of symmetry.

3. The toroidal theorem states that the velocity of the form $u = \bigtriangledown \times r\psi$ are incapable of generating magnetic field if λ is a function of $\mid r \mid$ only, where r is a position vector. This theorem has a very important geophysical implication, which states that in order to have a

magnetic field, a radial component of velocity must be maintained over periods of the order of magnetic decay time[Bus83].

2.3 Seismology

Seismology is the study of earthquakes and the elastic waves that move through the planet. It may also include the aftermath of an earthquake, which can range from Tsunamis to simple aftershocks. Earthquakes are known to produce two types of waves: **P waves**, where **P** stands for pressure or primary, are longitudinal waves which travel through liquid and solid medium. **S waves**, where **S** stands for shear or secondary, are transverse waves that can only travel through solid medium[sei]. As these waves travel at different velocities, it is possible to detect them and hence deduce the internal structure of our planet.

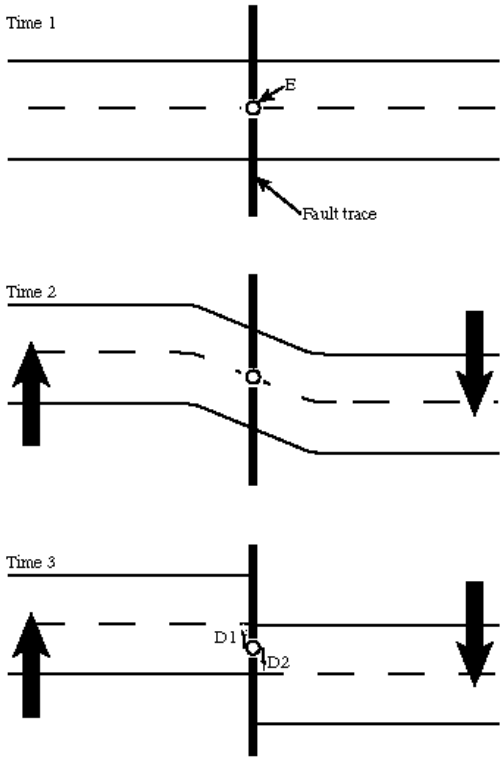

Figure 2.2: Elastic rebounding in tectonic plates. (Courtesy: Scitable by Nature education)

2.3.1 Elastic Rebound Theory

Previous observations have led us to believe that the surface of earth is not completely rigid. When tectonic plates move towards each other in places where they are not locked along fault lines, the surface tends to change shape and shows signs of bending/ rising. This change of shape is responsible for storing energy in that particular region, the same energy which will be later released during an earthquake. When this accumulated strain is greater than the strength of nearby rocks, it snaps like an elastic, and an earthquake occurs. The time difference between T1 and T2 can range from a few months to a few centuries, and between T2 and T3 it is only a few seconds. The pictorial representation of elastic rebound theory is shown in figure 2.2.

2.4 Earthquakes

A sudden shaking of earth's surface due to a movement of the underlying tectonic plates is termed as an earthquake. For thousands of years, we have seen how destructive an earthquake can prove to be, based on the sheer area that it affects, and other calamities that are then caused as a result of the earthquake has been well documented and studied. Major examples in recent past are Tsunami of 2004 which was a result of a 9.2 Magnitude earthquake of the coast of Sumatra and the Fukushima nuclear disaster and Tsunami as a result of Tohoko earthquake with a magnitude of 9.1.

2.4.1 What causes an earthquake?

There has been a long-standing consensus in the scientific community about the structure of earth's crust and mantle. It is believed to be made of several thin and rigid slices or plates which are constantly in motion albeit extremely slowly and often collide into each other to cause shocks on the surface which we call as earthquakes. There is an overwhelming majority of earthquakes that have been recorded along the proposed fault lines which only goes on to support the claims in support of the tectonic theory of earth's crust. There are six major plates which are named after the continents that they are embedded in, namely, North America, Africa and several small ones which play an equally important role in shaping the earth lithosphere.

2.4.2 Detecting and Measuring an Earthquake

Detection of an earthquake and measurement of the vibrations is done using a device called **seismograph**. The amplitude measured defined on a scale called the **Richter scale** which is synonymous with measuring the magnitude of an earthquake[dic]. Theoretically, the magnitude can be any numerical value, but no earthquake has been recorded with a magnitude of more than 9.5. Moreover, it is believed that an earthquake of a magnitude greater than 11 will release sufficient energy to split the planet into two halves. This is a logarithmic scale so, with an increase of just one magnitude, ten times greater energy is released during the event.

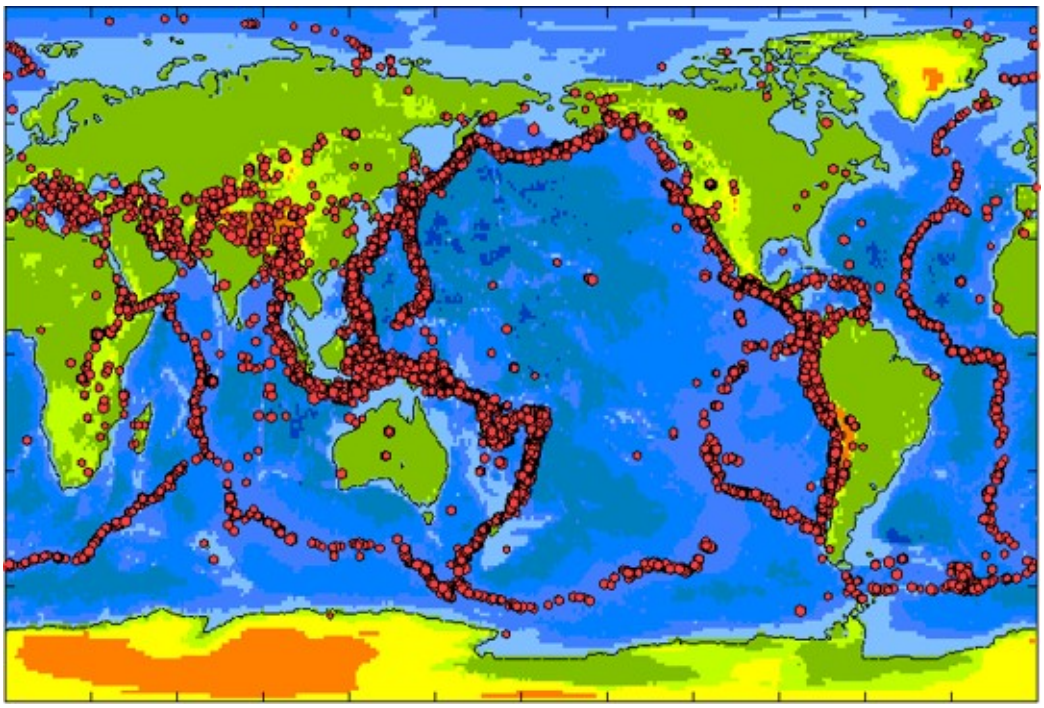

Figure 2.3: Plot of earthquakes over a 100 years. Clearly showing the concentration along the fault lines. (Courtesy: USGS)

2.5 Atmospheric effects

While observing cosmic ray flux incident on earth, it is important to consider atmospheric effects, mainly temperature to fully understand formation and decay of nuclei that cosmic rays are composed of. Atmospheric density varies with altitude as shown in the figure 2.4, which means fewer particles available for collision for incoming cosmic rays. When

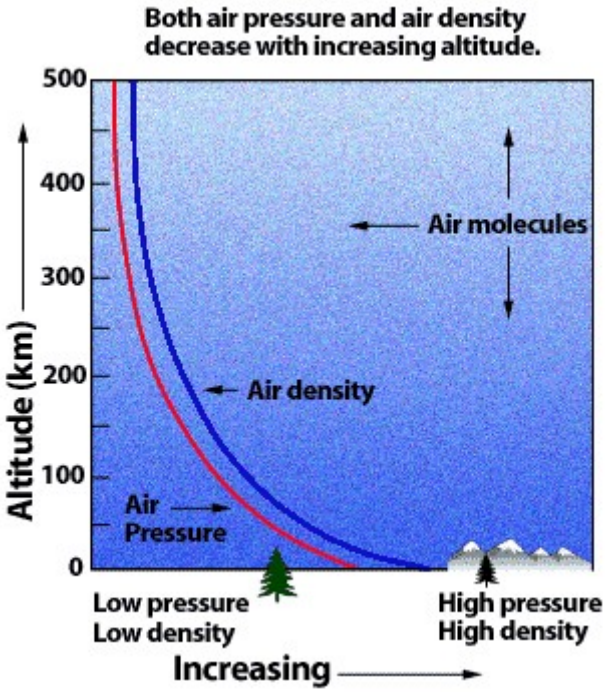

Figure 2.4: Variation in atmospheric parameters.

looking at temperature variation with time, GRAPE3 [gra] experiment collected data for 6 years, whose results will be discussed later.

Chapter 3

The Sun

3.1 Sun

Sun is the only star of our constellation. A nearly perfect spherical body made up of hot plasma with a core temperature estimated to be of the order of 10^7K, the surface temperature of 5770K and a coronal temperature of about 5×10^6 K. The name sun comes from the old English word sunne which means south. The Latin term ”sol” is also used in adjectival form ”solar” to denote anything that has to do with the sun, for example, solar activity, solar eclipse, solar flares etc. The distance of the sun from the earth is about 150,000,000 km, which is also defined as 1 Astronomical Unit(AU).

Based on the spectral classification of stars, the sun falls in the category of G-type main sequence and is also classified as a yellow dwarf because of increased intensity in the yellow, green portion of the visible spectrum.

3.2 Solar Phenomenon and Solar Cycle

Solar phenomenon is the collective term of all the events that happen either on the surface of the sun or are caused due to some event that took place on the sun. These can be of several forms such as solar winds, coronal mass ejection (CME), solar flares, sun spots etc. These events are believed to be generated due to the helical dynamo which is near the centre of the sun. This dynamo generates strong magnetic fields which then cause the said events. Moreover, near the surface, there is a chaotic dynamo which generates weaker magnetic field fluctuations.

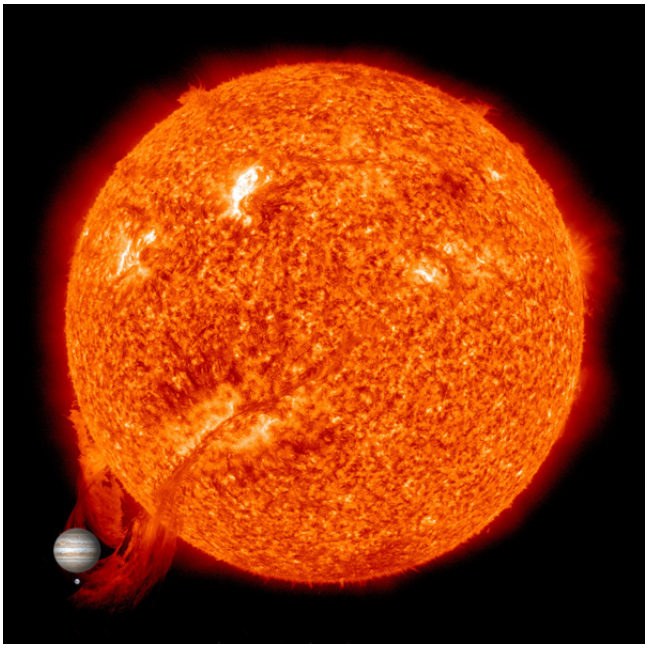

Figure 3.1: Solar prominence, which may ultimately breakdown to give rise to a CME. Images of Earth and Jupiter are added for comparison.(Courtesy:NASA Goddard Space Flight Center)

These solar events are so intense that they can be easily observed from the earth and astronomers have recorded coronal mass ejections and sun spots for hundreds of years. This extensive recording of data has shown to us that these solar events follow a pattern of sorts where solar activity fluctuates from a maximum to a minima value meanwhile undergoing a polarity reversal in the process. This cycle is about 11 years long with the actual range being from 10-14 year long. This solar cycle is responsible for modulating the flux of solar radiation, solar winds etc. In these 11 years of the solar cycle, the polarity of the sun also reverses its direction where magnetic north pole shifts to the geographic south pole and magnetic south pole shifts to the geographic north pole. This reversal of polarity only occurs during the minima phase of solar activity when new spots begin to form at higher latitudes.

3.3 Sunspots

It was Galileo who, using his telescope, first observed darker regions on the surface of the sun. Since then we have seen significant advancements in the understanding of the formation and subsequent disappearance of sunspots. These are the cooler darker regions

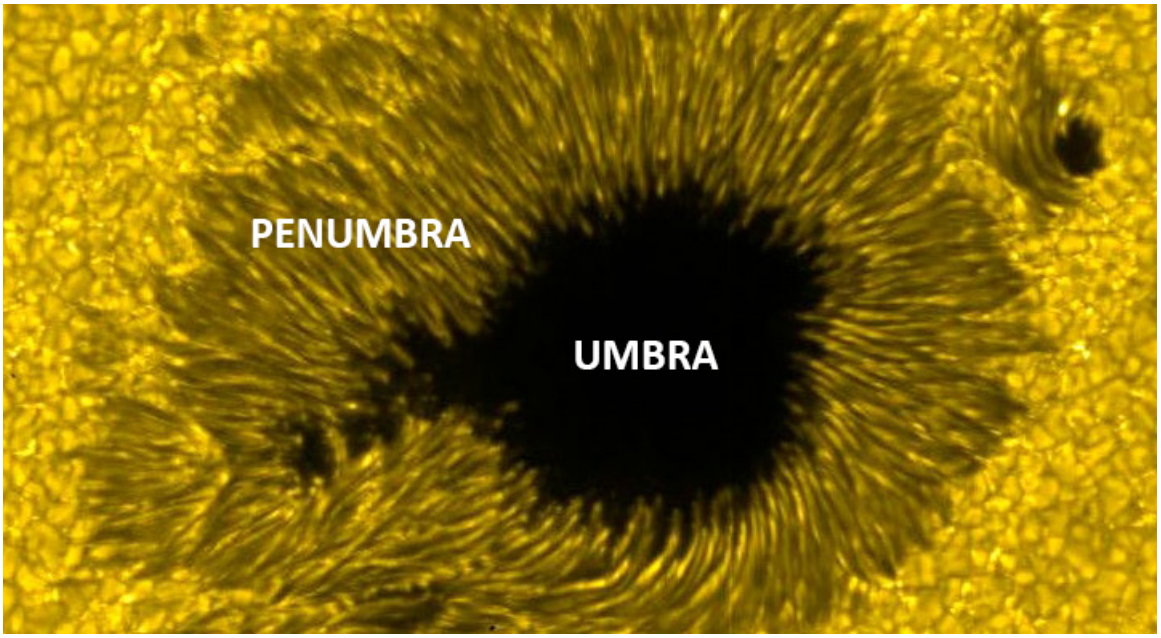

Figure 3.2: A sun spot showing the darker Umbra and surrounding Penumbra region.

near the surface of the sun which are temporarily formed due to inhibition of convection in the region due to formation of a magnetic dipole nearby. The number and frequency of sunspots also follow the solar cycle, and over a period of about 11 years, the number goes to maximum value from minimum and then back to minimum[Sva13]. The location of sunspot formation is also periodic, again with an 11-year cycle. Individual sunspot does not change its location after formation, but the next sunspot is likely to be formed at a lower latitude till they reach the equator. As the cycle comes to completion after reaching the equator, at approximately $\pm 40^o$ of the equator a new cycle starts to take shape. It is at the intermediate latitudes that we observe the maximum number of sunspots during the solar cycle.

The central darker region of the sunspot is called as an **umbra** and can be up to 30,000 km in diameter. The surrounding region which is reminiscent of a filament-like structure is called as a **penumbra** which is less dark as compared to the umbra. Moreover, this threadlike structure also supports the presence of strong magnetic field lines in the region. The idea of calculating the sunspot number was conceived by Rudolf Wolf in 1848 who gave the following equation:

$$R = k(10g + s) \tag{3.1}$$

R is the relative sunspot number, s stands for number of individual spots, g for the number of sunspot groups, and k varies with location and instrumentation (also known as the

observatory factor or the personal reduction coefficient K)[Fri16].

3.4 Interplanetary Magnetic Field

Interplanetary Magnetic Field(IMF) or Heliospheric Magnetic Field(HMF) is the part of the solar magnetic field which traverses across the solar system with the solar winds. This magnetic field component is thought to be fixated with the plasma in outer space. Sun's rotation and outward movement of the field gives rise to an interesting spiral pattern which can be described as water coming out of a rotating sprinkler or a ballerina's skirt. Mathematically this is an Archimedean spiral and specifically known as the Parker spiral.

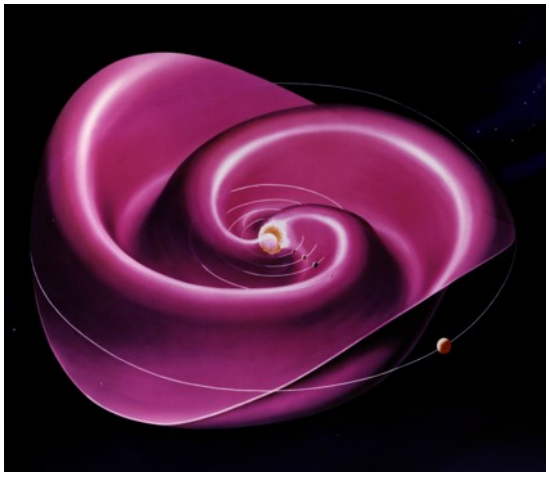

Figure 3.3: A representative diagram of Interplanetary Magnetic Field.(Courtesy: NASA)

This Parker spiral shape of the solar winds changes the shape of the magnetic field in outer space from poloidal to toroidal, i.e. pointing in North-South direction to pointing towards the equator. This also results in the amplification of magnetic field strength in outer space. Moreover, the Parker spiral is also believed to cause the differential rotation of sun. The equator rotates faster(27 days) as compared to the poles(35 days). It is important to note that the polarity of the sun is not constant and it flips every solar cycle thus flipping the entire magnetic field with it.

Chapter 4

Experiments

4.1 Ongoing Major experiments

Current experiments in the field of cosmic rays are mostly about observing and measuring the flux of incoming radiation. Most of the scientists attempt to study how this incoming radiation plays a role in processes that take place on earth and what information can be extracted from these about their origin. Studying the cosmic rays is vital to search for origins of the universe and how celestial bodies form. There are several major experiments on a wide variety of locations and landscapes where detectors have been set up to measure the incoming flux of cosmic radiation. We will have a look at three important ongoing experiments and the methodology that they have used along with the breakthrough results that have been hypothesised as a part of these.

4.1.1 ARGO-YBJ

ARGO-YBJ is a detector setup in Tibet at an altitude of 4300m m.s.l. The main aim of this experiment is to study the cosmic radiation at energy threshold of about 100 GeV by detection of small air showers at the Yangbajing Laboratory with help of an array of detectors. It has been about ten years since this full coverage EAS detector has been operational. This detector in unique as it serves two purposes:

- A γ ray telescope with a wide field view operating in the TeV energy region.
- A high-resolution detector to observe Cosmic Rays in the range of few TeV up to 10 PeV.

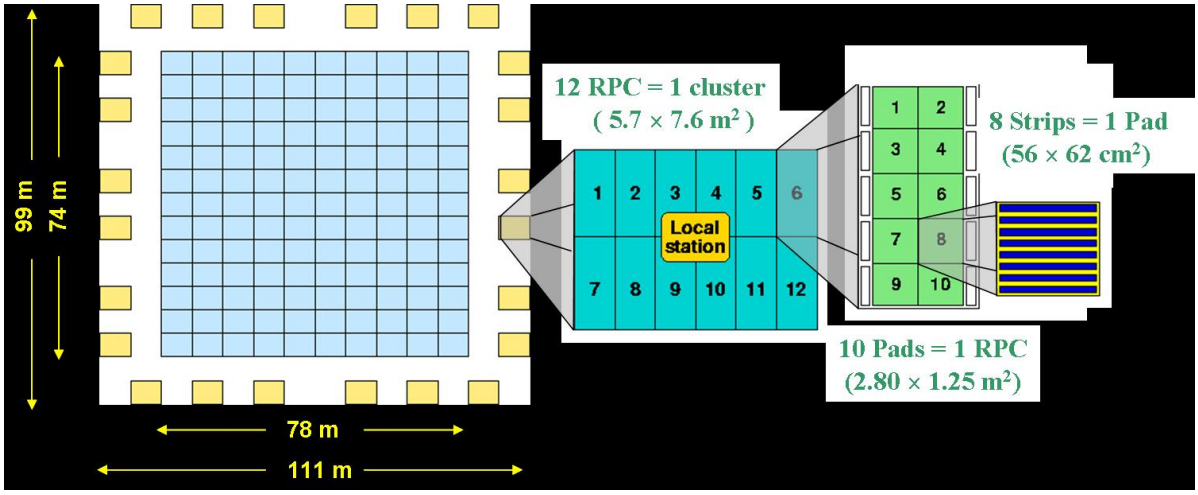

Figure 4.1: Schematic of ARGO-YBJ detector showing the RPCs. (Courtesy ARGO-YBJ).

4.1.2 GRAPES-3

GRAPES-3 (Gamma Ray Astronomy PeV EnergieS phase-3) experiment is located in Ooty, India at an elevation of 1900m. This experiment was started as a collaboration between Tata Institute of Fundamental Research, Mumbai and Osaka city University, Japan. This experiment aims to detect cosmic rays with a large area muon detector and an array of air shower detectors.

Figure 4.2: Array of air shower detectors at Ooty, India. (Courtesy: GRAPES-3)

It operates in 4 astrophysical settings so as to probe cosmic rays:

- 100 MeV in atmospheric electric through muons.
- 10 GeV in Solar system through muons.
- 1 PeV in our galaxy through nuclear composition of cosmic rays.
- 1 EeV in nearby universe through measurement of diffuse γ - ray flux.

The main objectives of the GRAPES-3 Experiment are:

- Attempting to find the origin of $> 10^{14}$ eV cosmic rays and to study their acceleration and propagation.
- Explanation of the feature "knee" in the cosmic ray spectrum.
- Observe extremely high energy cosmic rays (10^{20} eV) in the universe.
- Studying the γ ray in TeV energy range, coming from neutron stars.
- Observing the incoming radiation from Sun and its effects on Earth.

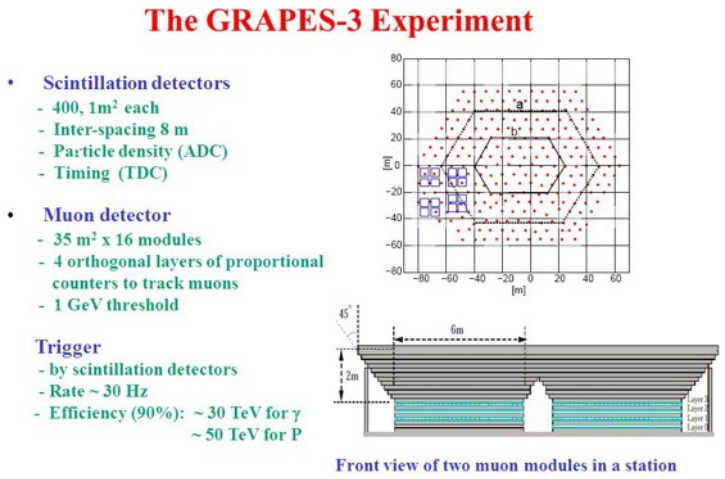

Figure 4.3: Detector used at GRAPES-3 experiment. (Courtesy: GRAPES-3)

4.1.3 AMS-02

AMS-02 (Alpha Magnetic Spectrometer) is set up on board International Space Station since 2011 as an external module. It is a particle physics detector with very high precision and wide range measurement capabilities. The primary task of this experiment is to look

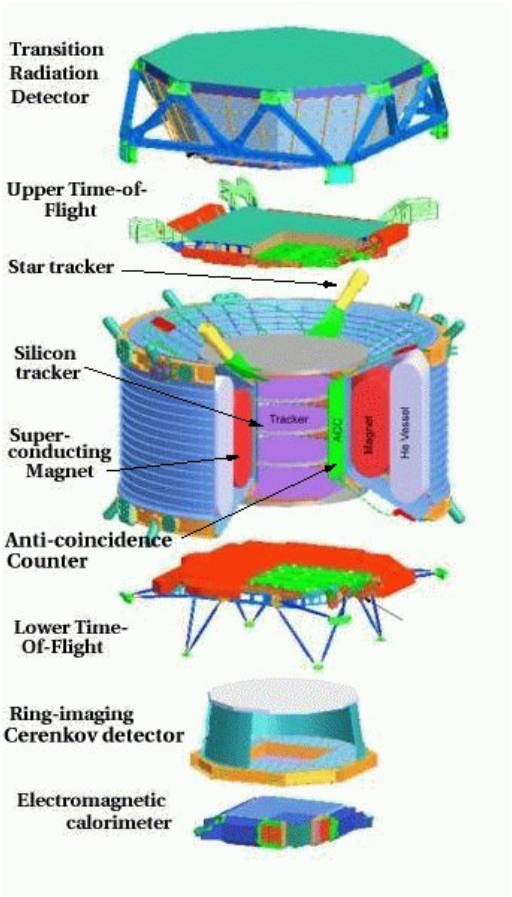

Figure 4.4: Expanded AMS detector. (Courtesy Benjamin Monreal)

for evidence of primordial antimatter and the presence of dark matter in the universe. This is the first instance of such a large magnetic spectrometer being installed in outer space. The biggest advantage of being setup in space is that observations made are unaffected by collisions or decay that incoming particles may undergo once they enter the earth's atmosphere.

Two different magnetic systems have been developed for the project. First one is a permanent magnet made up of 6000 Ne-Fe-B pieces which are assembled after careful magnetisation. This magnet was sent up ISS in 1998, and it has been designed to operate at ambient temperature. The second system is a superconducting magnet which operates at 1.8K. It is built using aluminium matrix to stabilise 14 coils of superconducting Niobium wire. The extremely low temperature of 1.8K is maintained by slow evaporation of 2500L superfluid Helium.

The two systems are designed in such a way that they share the same magnetic field configuration. This is called a "*magic ring*". The reason behind this configuration is to have neg-

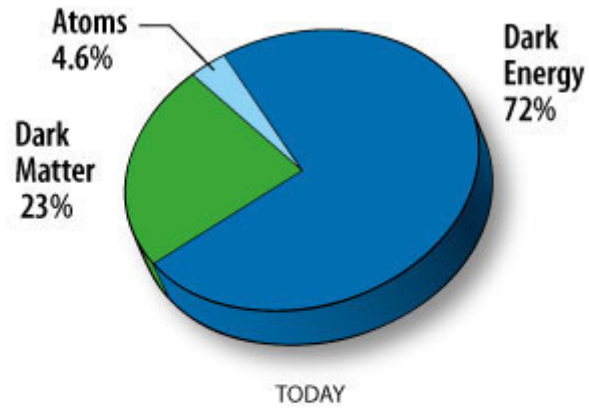

Figure 4.5: Ratio of Dark Matter

ligible net dipole moment of the two magnetic systems to avoid any coupling with earth's magnetic field lines. If coupling were to happen, it would disrupt the orbit of ISS. Hence making it important to ensure almost nil dipole moment.

Four main objectives of AMS-02 are:

- Search for Antimatter.
- Search for Dark matter and Dark energy.
- Detection of "Strangelets".
- To study the composition of Cosmic rays and Cosmic ray flux.

Chapter 5

Mathematical Methods

5.1 Calculation Methods

5.1.1 Correlational Analysis

In simpler terms, correlational analysis is just a comparison of two data sets. The value for correlational coefficient goes from -1 to +1 where extremities correspond to complete correlation or complete inverse correlation, whereas values closer to 0 demonstrate a diminishing correlation between the two data sets. The limitation with this computation of correlation is that it can only be used for linear correlation. Non-linear dependencies are not computable by this method.

There are four main types of correlational techniques that are used. Each of them is discussed below:

- **Pearson Correlation** : This is the most widely used analysis of linearly dependent data. It is important to note that both variables should be normally distributed. The formula used is:

$$r = \frac{N\Sigma xy - \Sigma(x)(y)}{\sqrt{N\Sigma x^2 - \Sigma(x^2)[N^2 - \Sigma(y^2)]}} \tag{5.1}$$

  Where,

  r= Pearson coefficient

  N= Number of Observations

  Σ xy= sum of the product of paired values

  Σx = sum of x values

Σy = sum of y values

Σx^2= sum of squared x values

Σy^2 = sum of squared y values.

- **Kendall rank correlation**: This analysis is done for measuring the strength of dependence between two variables by means of a non-parametric test. The formula used for the text is as shown below:

$$\tau = \frac{n_c - n_d}{\frac{1}{2}n(n-1)} \tag{5.2}$$

Where, n istands for total number of values, n_c are the values ordered in the same way, also called as concordant and n_d are the values ordered differently, also called as discordant.

- **Spearman Rank Correlation**: This is a non-parametric test to measure the degree of association. It does not consider any assumption about the data and is most appropriate when the variables are measured on similar scales. The formula used for Spearman rank correlation is:

$$\rho = 1 - \frac{6\Sigma d_i^2}{n(n^2-1)} \tag{5.3}$$

Where ρ is the Spearman coefficient, n is the total number of cases and d_i is the difference within the paired ranks.

5.1.2 t-test

The t-test is a comparison of two normally distributed data. It tells us whether there is any significant difference between the means of the two data sets[NS14]. We used a specific case of Welch's t-test, where sample size can be equal or unequal, and variance are unequal. This is often termed under unpaired t-tests or independent sample tests.
The formula used for a Welch's t-test is:

$$t = \frac{\bar{X}_1 - \bar{X}_2}{\sqrt{\frac{s_1^2}{N_1} + \frac{s_2^2}{N_2}}} \tag{5.4}$$

Where, $\bar{X}_i$, s_i and N_i are mean, variance and size of the i^{th} sample respectively.

5.1.3 Time Series

A sequence of data points ordered successively is called a time series. It tracks the value of said parameter over some time and measures changes in it. It is important to note that is the type of data is discrete and numerical in nature. Time series analysis is the technique that is performed on the given data to extract information. It may be used to find a correlation between any two different data sets, or even to forecast the movement of the parameter towards a certain value. A time series is often denoted as shown:

$$X = \{X_1, X_2, X_3, ...\} \tag{5.5}$$

The simplest way to analyse a time series is to begin with a basic line graph.

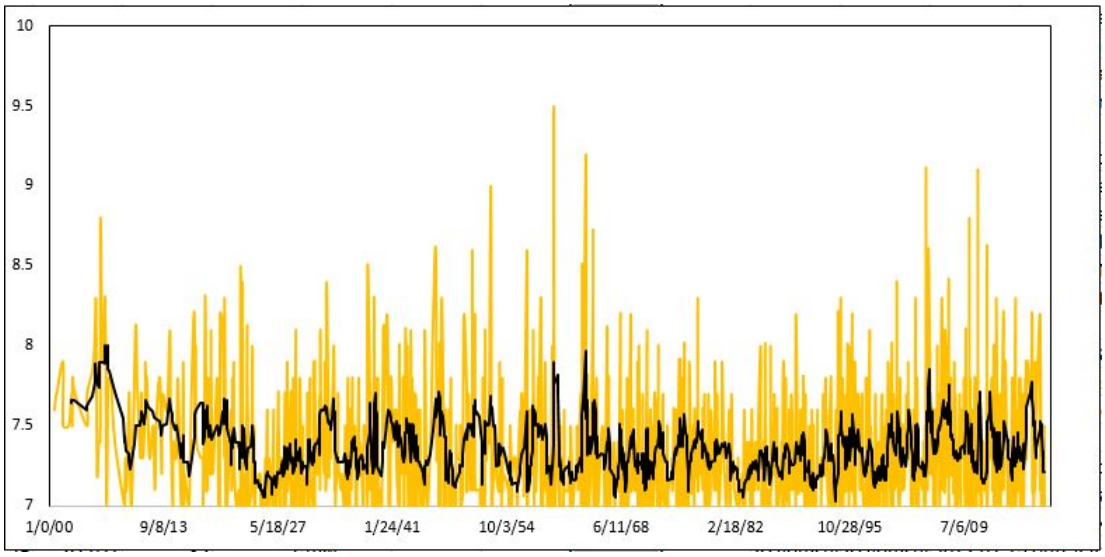

Figure 5.1: A time series of earthquakes from 1900 onwards. The black line represents a moving average of 7 years.

5.1.4 Fast Fourier Transform

A **Fast Fourier Transform** is an algorithm to compute the discrete Fourier Transform for a sequence. In most cases, it takes a signal in time or space domain and converts it to the frequency domain. The discrete signal is obtained when the original signal is decomposed into components of different frequencies.

Chapter 6

Observations

6.1 Solar Cycle and Cosmic ray Flux

6.1.1 Solar Cycle

Yearly and Monthly average number of sunspots were taken from SDIC and then plot as a time series function. We observed the pattern of 11 year cycle in solar activity as shown in the plot below: The graph clearly shows the cyclic nature of sunspot number and hence

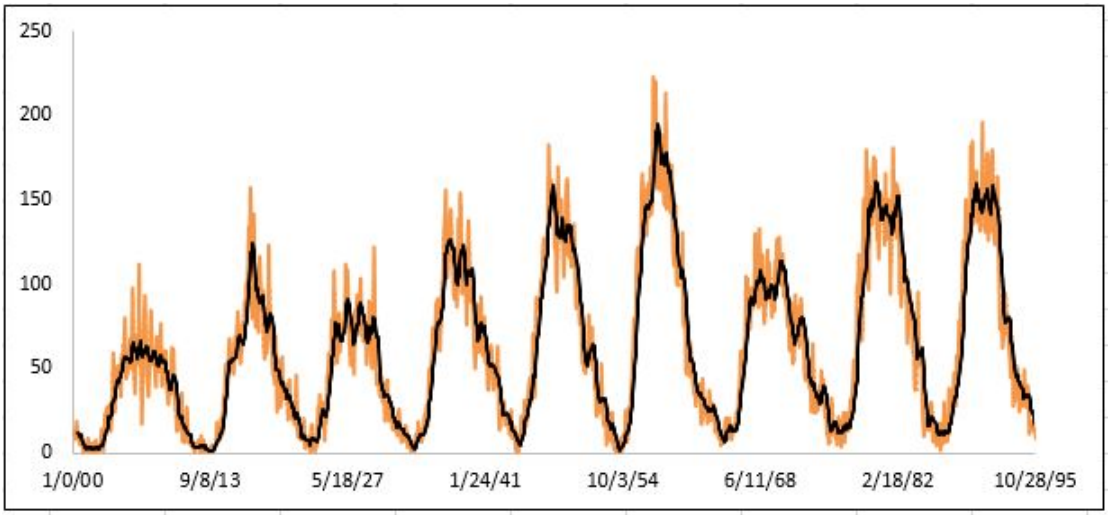

Figure 6.1: Monthly Average of Sun spot Numbers.(1900-1995).

the solar activity. The minimum duration for an individual cycle was 9 years where as maximum was about 14 years. These cycles are in close proximity to the 11 year average which is generally defined as the duration of a typical solar cycle. Moreover as our data points are discrete and ordered in a time sequence this is an example of time series plot.

6.1.2 Muon Flux

Values for flux were taken from AMS detector observations of incoming electrons. Energy threshold for the observation was limited to $< 15GeV$. The source for this data was chosen to be the AMS-2 detector because of its location which is conveniently situated several hundred kilometers above the surface. Hence the disturbances due to atmospheric intervention are least. The mean value for e^- flux was calculated to be:

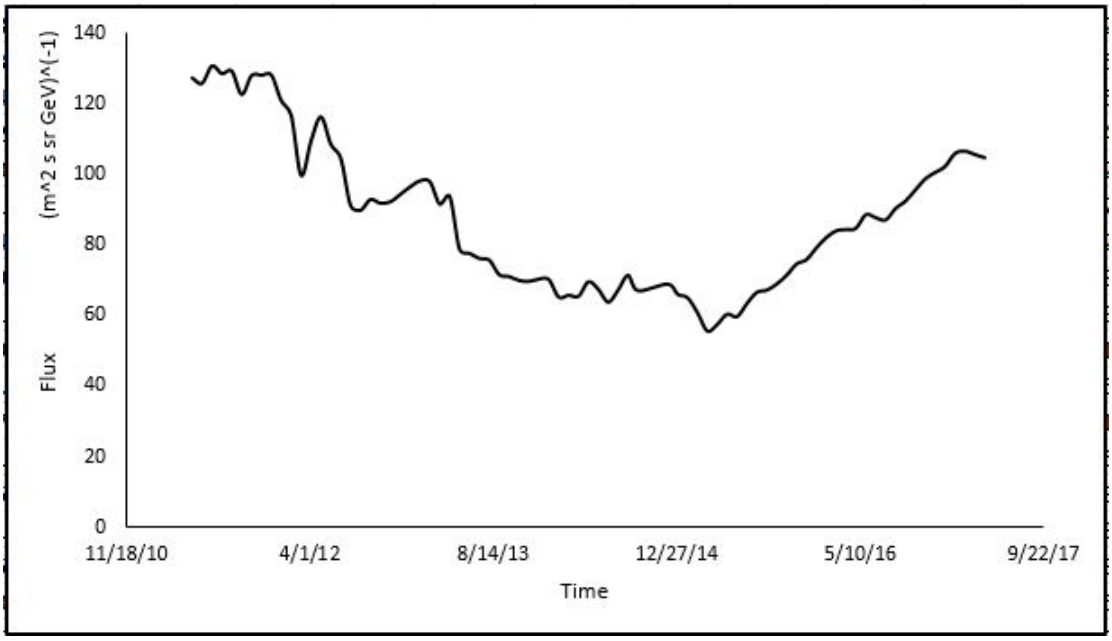

Figure 6.2: Flux when measured between the energy range 1.01 GeV - 15 GeV.

$$\bar{x} = 88.05(m^2 * s * sr * GeV)^{(-1)} \tag{6.1}$$

Where as the standard deviation:

$$\delta = 21.02(m^2 * s * sr * GeV)^{(-1)} \tag{6.2}$$

Shown below is the flux of neutrons at energies $< 1GeV$. This was collected over a period of more than 50 years as hourly data by the detector setup at Kiel. We can clearly see the cyclic nature of the data series hinting at the periodicity in flux values.
The mean value for μ flux was calculated to be:

$$\bar{x} = 5979.44(m^2 * s * sr * GeV)^{(-1)} \tag{6.3}$$

Where as the standard deviation:

$$\delta = 331.17(m^2 * s * sr * GeV)^{(-1)} \tag{6.4}$$

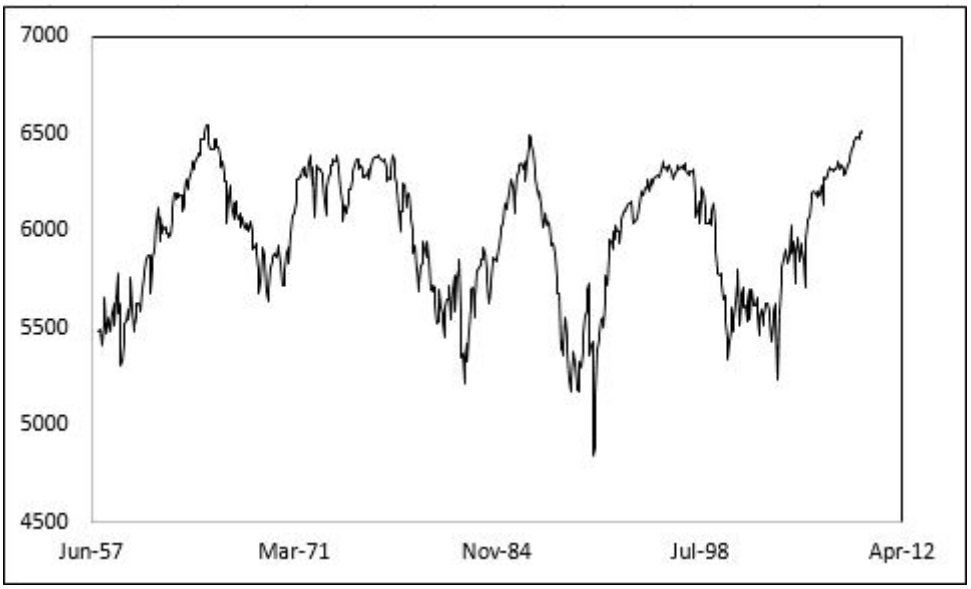

Figure 6.3: Observed flux of cosmic rays averaged monthly.

6.1.3 Comparing the Two Series

As already stated, the two data sets are representative of time series. Moreover the data points are discrete and numerical in nature, therefore we used **Pearson Correlation** analysis so as to find any dependencies of the two series on each other. We also plot the two time series. For the purpose of this calculation we chose the maximum time series of flux values and exactly same for the sun spot number.

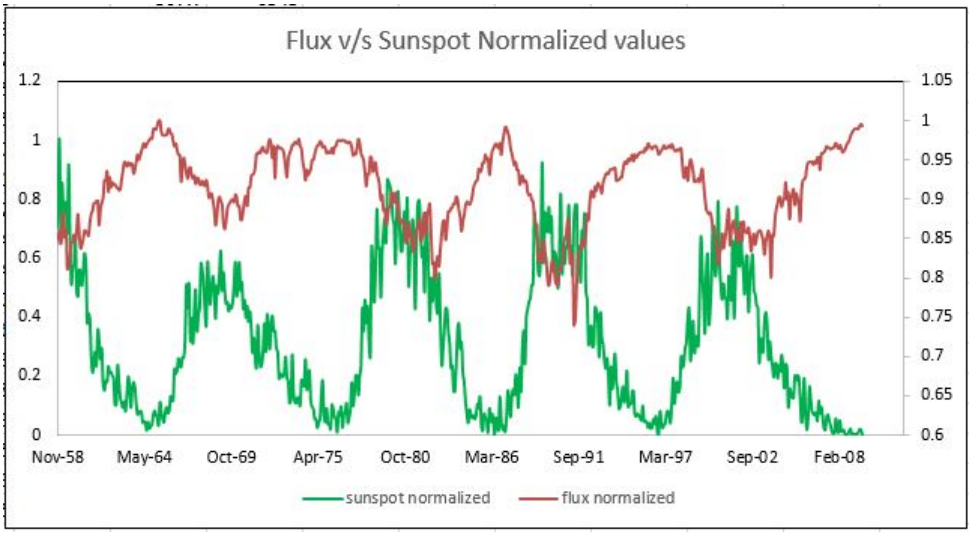

Figure 6.4: Sunspots v/s Cosmic ray flux time series normalised to 1.

Correlation coefficient between time series of figure 6.1 and figure 6.3 was calculated to be $r = -0.779$ using equation 5.1. This value shows a very strong negative correlation

between the two values. As seen from the graph and calculated value, flux of incoming particles was highest during the times of sunspot minimum and vice versa. Where as when the flux of particles with energies in the range 1.01-15GeV was compared with the Sun spot number, the correlation coefficient varied in the range of $(-0.2 - +0.2)$ calculated in a case by case basis with bins of 1 GeV range and also as a cumulative flux over the complete range of energies.

6.2 Muon and Temperature

6.2.1 Muon and Temperature Data

For the following analysis [A$^+$17] of variation in Muon intensity, GRAPES-3 was taken to be the reference. The location of GRAPES-3 detector is lowest in altitude when compared to the other two major experiments and therefore the atmospheric effects are most pronounced.

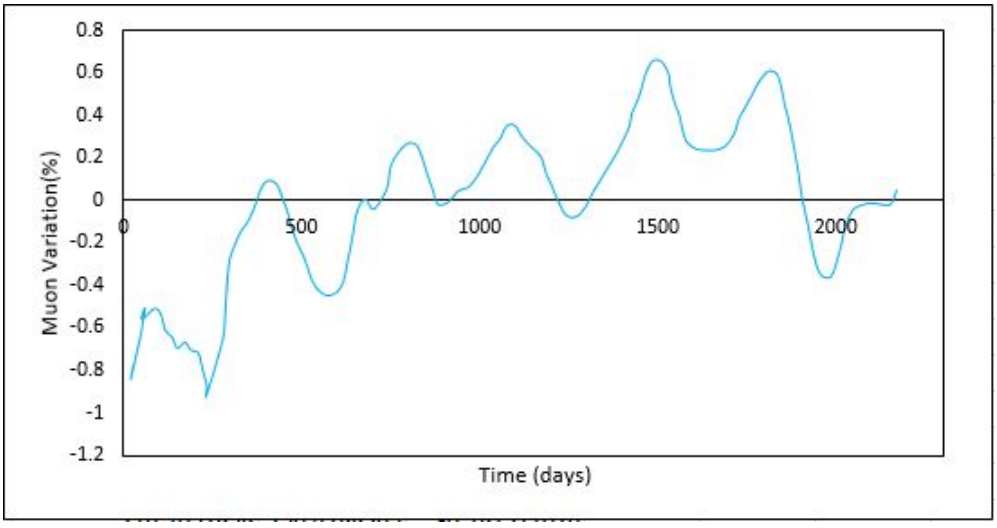

Figure 6.5: Variation in Muon Intensity (60 days moving average).

The variation in muon intensity was relatively small, temperature was hence taken to be as effective temperature where altitude changes were taken into account.

$$T_{eff} = \frac{\Sigma e^{\frac{-x}{\lambda}}(x)\Delta x}{\Sigma e^{\frac{-x}{\lambda}}\Delta x} \tag{6.5}$$

'x' stands for atmospheric depth to factor in the pressure changes, λ is attenuation length for hadrons and temperature at the height x is T(x). The attenuation length has been previously

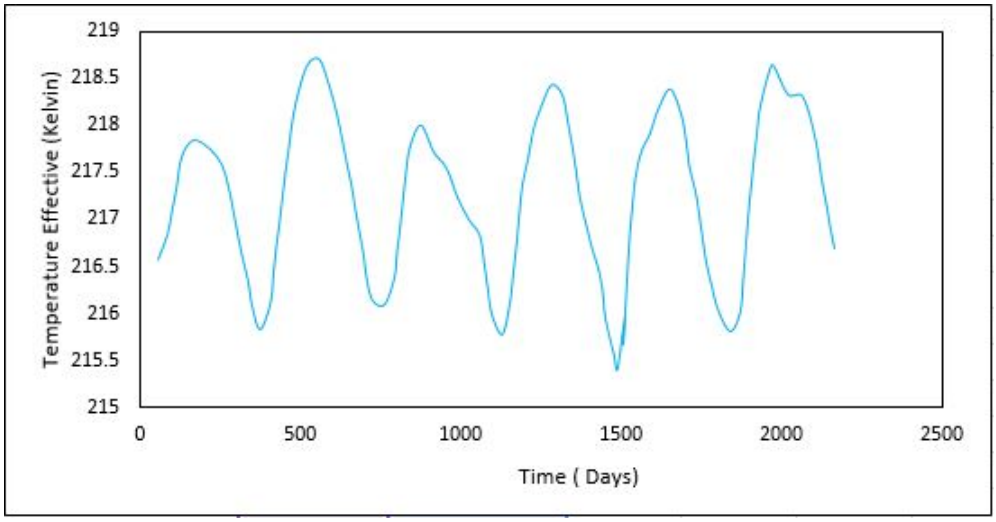

Figure 6.6: Variation in Temperature (60 days moving average).

estimated to be in the range of $80 - 180 gcm^{-2}$. The central value of $120 gcm^{-1}$ was chosen for the purpose of this calculation. Moreover as the data was clearly periodic, it was filtered by a narrow band filter W(f) to only choose the frequencies centered at 1 cycle per year or 0.00295 cycle per day and $\Delta f = 0.00035 cycle per day$ was chosen to filter the data.

$$W(f) = \begin{cases} 1, & \text{if}, |f - f_c| \leq \Delta f \\ \sin \frac{\pi}{2} \frac{|f-f_c|}{\Delta f}, & \text{if}, \Delta f \leq |f - f_c| \leq 2\Delta f \\ 0, & \text{if}, |f - f_c| \geq 2\Delta f \end{cases} \tag{6.6}$$

Then this filtered frequency was analysed by performing an inverse fast Fourier transform so as to get the data back in time domain. These data series were then plotted against time. Dependency of muon variation was also calculated on temperature data by measuring the distance of individual values from the respective mean values.

Muon variation is related to the temperature change by the following equation:

$$\frac{\Delta R_{3h}}{< R_{3h} >} \times 100 = \alpha_t \times T \tag{6.7}$$

Here R_{3h} is the measured muon rate over an interval of 3 hours, α_T is the temperature coefficient and ΔT is the change in temperature. The graph 6.8 was then used to estimate the coefficient α_T which was found to be $0.17\% K^{-1}$.

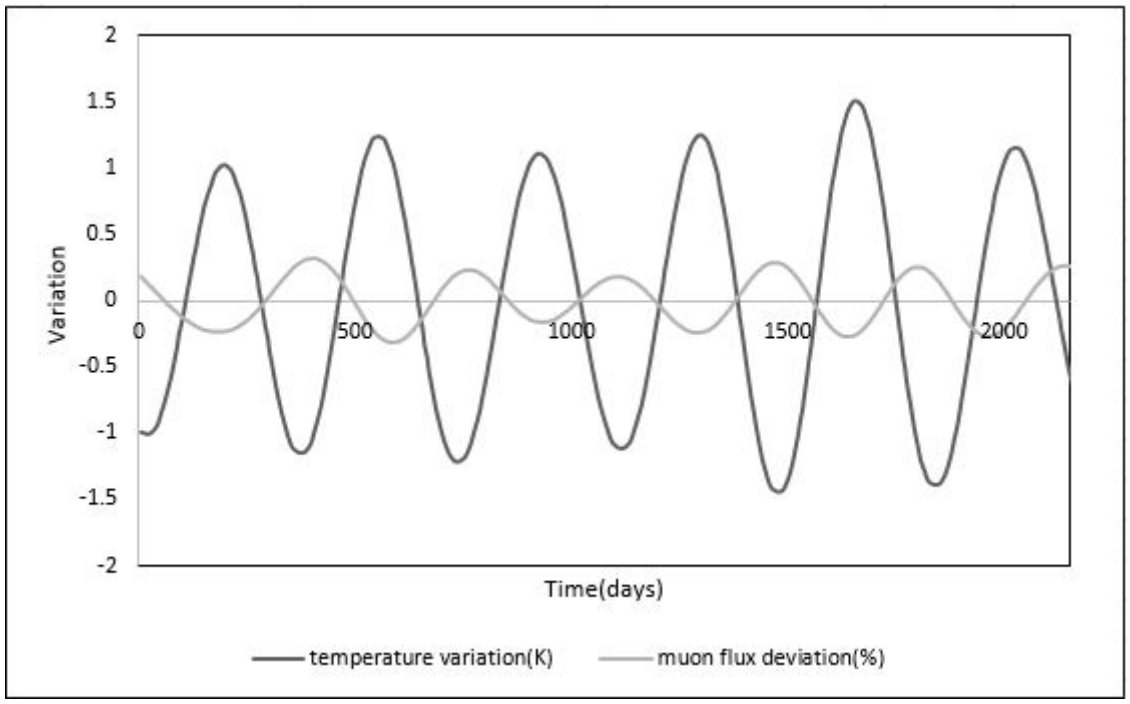

Figure 6.7: IFFT plot for muon variation and temperature change measured in time domain.

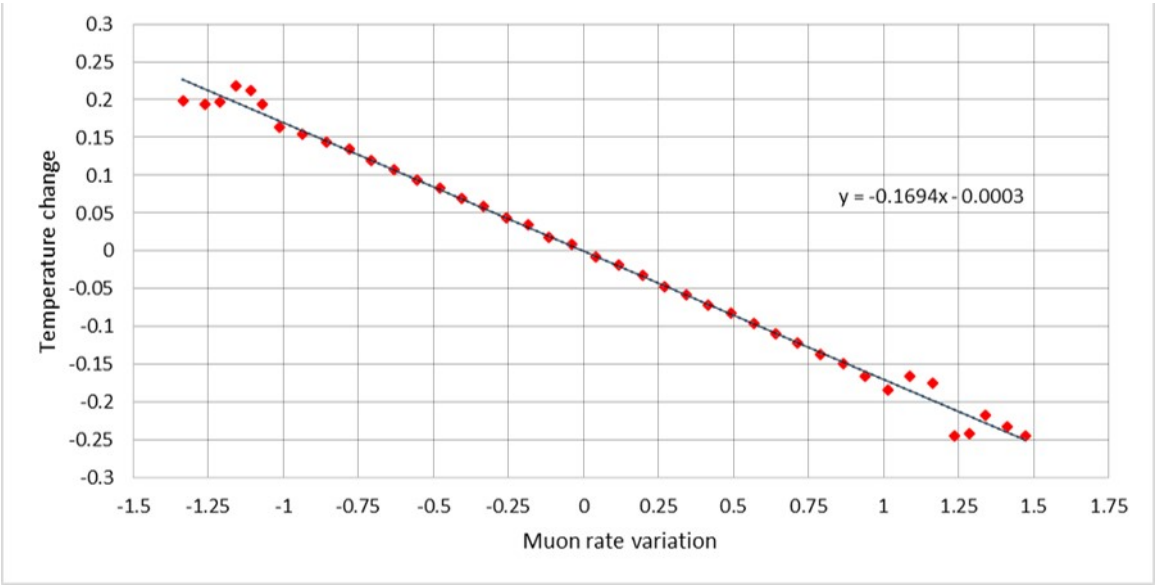

Figure 6.8: Muon variation dependence on temperature, relative to the mean values

6.3 Earthquake Data

For the purpose of next calculation, we filtered the available earthquake data since 1900 onward and limited to earthquakes with a magnitude of 7 and above on the **Richter scale**. A total of 1376 events were recorded and ordered in a yearly fashion so as to obtain the yearly average values. The plot for earthquake time series was obtained as shown in the figure 5.1. The plot for yearly number of earthquakes was obtained as shown below:

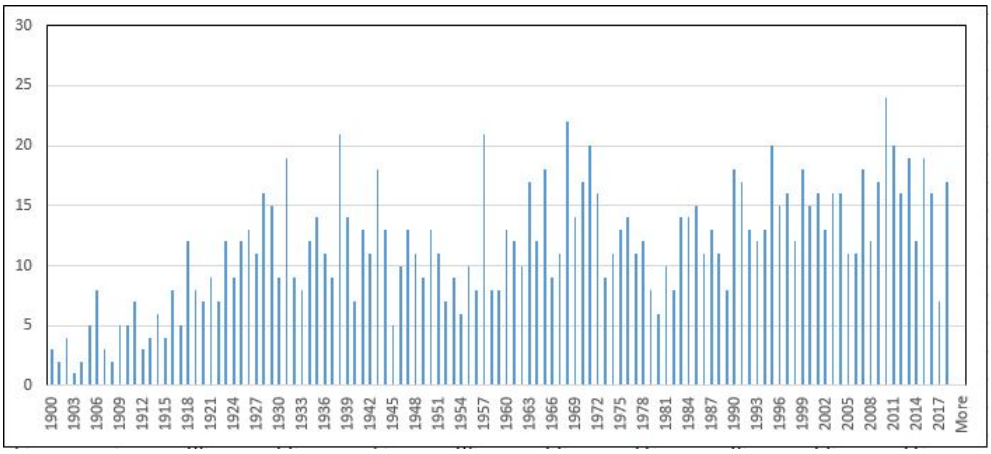

Figure 6.9: Frequency of ≥ 7.0 Magnitude earthquakes between 1900-2018

We grouped the available data according to the known Solar maximum years and ordered them with respect to time difference from the maximum[OBG$^+$06]. Same process was repeated with the obtained sun spot numbers and both the series were then plot together as shown below:

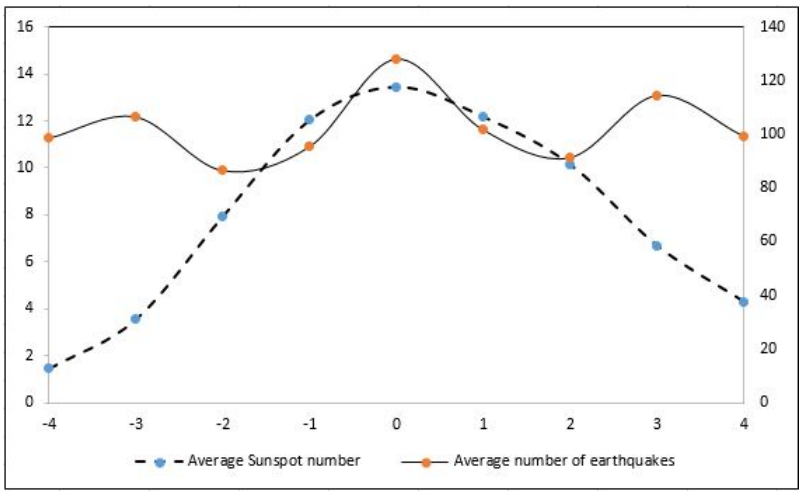

Figure 6.10: Yearly average number of sunspots and earthquakes above 7.0 magnitude. X-axis was the time relative to the solar maxima.

The global maxima of earthquake occurrence coincides with the maxima of sun spot number. To verify the statistical signifance of this result we used the **Welch's t-test** (equation 5.4) which assumes the data to have unequal variances. Number of earthquake occurrence in solar maxima year (mean=15.3, variance=36.68, n=10) were first compared with total number of earthquakes (mean=11.6, variance=23.75, n=100).

t Stat = -1.875888745

P(T$\leq t$) one-tail = 0.045065592

t Critical one-tail = 1.812461123

P(T$\leq t$) two-tail = 0.090131183

t Critical two-tail = 2.228138852

The p value of 0.045 is well within the harder criteria for classifying the two data sets to belong to significantly different populations. In other terms, we can draw the inference that number of earthquakes in solar maxima years are influenced by some other factor as compared to all the earthquakes, which in this case is solar activity. When similar comparisons were made between the geomagnetic activity cycle and solar activity cycle a similar dependence was found. This suggests the action of same features on the geomagnetic activity and earthquake occurrence.

The results discussed above only strengthen our belief that earthquake occurrence is affected by changing solar activity. Moreover in a more specific scenario individual events can be analysed to look for any significant changes in solar activity preceding the event.

Chapter 7

Results and Future Prospects

7.1 Results

Our analysis provided strongly positive results correlating:

- Muon flux v/s Sunspot number (r = -0.779)

Our analysis provided evidence for a strong inverse correlation between sunspot number and muon flux which can be explained by the interference of tangled magnetic field with the cosmic ray particles[Hat15]. When solar activity is increased, magnetic structures start moving outwards in the solar system which then leads to a scattering of cosmic ray particles and a reduced flux in the inner solar system.
Moreover, the change in cosmic ray flux tends to lag behind the solar activity change. This is accounted by the preexisting models for galactic transportation of cosmic rays in the heliosphere[FP04].

- Moun flux v/s Atmospheric temperature (α_t=0.17%K^{-1})

The effects of temperature variation were not very pronounced hence careful selection and processing of data was required. We calculated the coefficient α_T to find the dependence of muon flux change with temperature variation. α_T was calculated to be $0.17\%K^{-1}$ for the attenuation length $\lambda = 120gcm^{-2}$. We looked for seasonal changes in the data meanwhile eliminating any variations that were caused by the sun. The flux of low energy muons shows an inverse correlation with temperature variation. As the atmospheric temperature rises, the fraction of muons that undergoes decay also increases. This may be caused as

a result of thermal expansion of atmosphere which in turn increases the path length for travelling muons[A$^+$17].

Studying seasonal changes is important as these corrections are essential to study the long term Cosmic ray variations. Use of FFT was helpful in the analysis as it helped us to eliminate the solar factors in our observations. An interesting result was that any correction that we calculated was independent of the chosen value of λ.

- Sunspot number v/s Earthquake occurrence

We could show that there exists a connection between seismic activity and solar activity. The frequency of earthquakes increases during the solar maximum and the energy released during an earthquake is also greater during that period[OBG$^+$06]. Data for past 100 years of earthquakes and sunspot numbers was analysed for calculations. We grouped our data set into years relative to sunspot maximum and then the frequency of earthquakes was observed. We see that this increase in earthquakes is also evident in the years ± 3 from the solar maximum year. This may be explained by a change in the polarity of sun, which then leads to an increase in solar winds and other such phenomena[Sim67].

If a prolonged experiment is done with direct observations and a specific case study of individual events to find the actual dependence of tectonic activity on preceding solar phenomena it will be significantly helpful in understanding if any earthquakes were triggered by the solar activity. If at all a model is formulated to predict the triggering of earthquakes by cosmic ray flux or incoming solar winds, it will prove to be of great scientific and social importance.

Bibliography

[A+17] K. P. Arunbabu et al., *Dependence of the muon intensity on the atmospheric temperature measured by the GRAPES-3 experiment*, Astropart. Phys. **94** (2017), 22–28.

[AK77] R. K. Adair and H. Kasha, *Cosmic Ray Muons*.

[Bus83] F H Busse, *Recent developments in the dynamo theory of planetary magnetism*, Annual Review of Earth and Planetary Sciences **11** (1983), no. 1, 241–268.

[dic]

[Ein05] Albert Einstein, *On the electrodynamics of moving bodies*, Annalen Phys. **17** (1905), 891–921, [Annalen Phys.14,194(2005)].

[FP04] S. E. S. Ferreira and M. S. Potgieter, *Long-term cosmic-ray modulation in the heliosphere*, The Astrophysical Journal **603** (2004), no. 2, 744–752.

[Fri16] Thomas K. Friedli, *Sunspot observations of rudolf wolf from 1849 – 1893*, Solar Physics **291** (2016), no. 9, 2505–2517.

[gra] *3 experiment*.

[Hat15] David H. Hathaway, *The solar cycle*, Living Reviews in Solar Physics **12** (2015), no. 1.

[Mon16] Paolo Montini, *Cosmic ray physics with ARGO-YBJ*, Nucl. Part. Phys. Proc. **279-281** (2016), 7–14.

[Nce12] Ncei.info@noaa.gov, *Noaa national centers for environmental information (ncei)*, Feb 2012.

[NS14] Geoffrey Norman and David Streiner, *Bare essentials*, Peoples Medical Publishing House, 2014.

[OBG+06] S. Odintsov, K. Boyarchuk, K. Georgieva, B. Kirov, and D. Atanasov, *Long-period trends in global seismic and geomagnetic activity and their relation to solar activity*, Physics and Chemistry of the Earth, Parts A/B/C **31** (2006), no. 1-3, 88–93.

[sei]

[Sim67] John F. Simpson, *Solar activity as a triggering mechanism for earthquakes*, Earth and Planetary Science Letters **3** (1967), 417–425.

[Sva13] Svalgaard, Leif, *Solar activity - past, present, future*, J. Space Weather Space Clim. **3** (2013), A24.